Chinese Chemical Letters 35 (2024) 108320

Contents lists available at ScienceDirect

Chinese Chemical Letters

journal homepage: www.elsevier.com/locate/cclet

Boosting the proton conduction in a magnetic dysprosium-organic framework by introducing conjugate NH_4^+-NH_3 pairs

Yi-Ping Qu[1], Qian Zou[1], Song-Song Bao, Li-Min Zheng*

State Key Laboratory of Coordination Chemistry, School of Chemistry and Chemical Engineering, Collaborative Innovation Center of Advanced Microstructures, Nanjing University, Nanjing 210023, China

ARTICLE INFO

Article history:
Received 23 December 2022
Revised 13 February 2023
Accepted 8 March 2023
Available online 11 March 2023

Keywords:
Metal-organic framework
Proton conduction
Ammonia adsorption
Metal phosphonate
Single molecule magnet

ABSTRACT

Metal-organic frameworks (MOFs) with inherent porosity and suspended acidic groups are promising proton conducting materials in water or aqua-ammonia media. Herein we report a new lanthanide phosphonate, namely, $Dy_2(amp_2H_2)_2(mal)(H_2O)_2{\cdot}5H_2O$ (**MDAF-6**). It possesses a 3D open-framework structure, and shows a high NH_3 adsorption capacity of 142.4 cm^3/g at $P/P_0 = 0.98$ at 298 K due to acid-base interaction. Interestingly, the proton conductivity of **MDAF-6-NH$_3$** is enhanced by five orders of magnitude compared to **MDAF-6** after 8.5 h exposure in saturated NH_3-H_2O vapor, indicating the importance of coexistent conjugate acid-base pairs of H_3O^+-H_2O and NH_4^+-NH_3 in promoting proton conduction. Magnetic studies of **MDAF-6** revealed slow magnetization relaxation under zero dc field, characteristic of single-molecule magnet behavior. This work provides not only a new multifunctional MOF material, but also a new strategy to improve proton conduction in aqua-ammonia medium.

Metal-organic frameworks (MOFs) with intrinsic porosity and tailorable surface chemistry are an emerging class of proton-conducting materials for clean-energy related applications [1,2]. In order to improve proton conductivity of the material, the proton carrier concentration and mobility must be increased. To this end, great efforts have been made in developing water-mediated proton conducting MOFs because water can offer conjugated acid-base pair of H_3O^+-H_2O and contributes to the construction of efficient proton-conducting pathway [3–7]. While the concentration of proton carriers can be increased by introducing acidic groups in the framework and/or acidic counterions and guests [8–12]. Besides water, NH_3 is also considered as a promising medium for proton conduction because of its similarity to water [13]. Recent reports have shown that exposing the material in NH_3-H_2O vapor can significantly increase the proton conductivity by 1–2 orders of magnitude [14–19]. However, it is unclear whether the coexistence of conjugate NH_4^+-NH_3 and H_3O^+-H_2O pairs can further enhance the proton conductivity. To answer this question, MOFs with good ability to adsorb ammonia and possessing structural stability in basic media are highly desired.

Metal phosphonates are known to exhibit high thermal and chemical stability because each phosphonate group can afford three oxygen atoms to bind metal ions [20]. The water stability of trivalent and tetravalent metal phosphonates is higher compared to monovalent and divalent metal compounds [21]. By selecting suitable metal ions and phosphonate ligands, porous metal phosphonates containing P-OH acidic groups can be designed and synthesized for ammonia adsorption and proton conduction [22–26]. Herein, we report a mixed-ligand dysprosium framework $Dy_2(amp_2H_2)_2(mal)(H_2O)_2{\cdot}5H_2O$ (**MDAF-6**), where amp_2H_4 is a pre-photodimerized 9-anthrylmethylphosphonic acid and $malH_2$ is malonic acid. The amp_2H_4 was chosen because it contains a large and flexible dianthracene group, which facilitates the formation of a 3D framework structure [27–29]. Dy^{III} ion was chosen because its trivalent state can improve the framework stability and its unique magnetic properties lead to multifunctional materials [30–36]. Indeed, **MDAF-6** shows a 3D open framework structure in which the uncoordinated P-OH group dangles over the channel surface. It exhibits excellent NH_3 adsorption capacity due to the acid-base reaction between NH_3 and P-OH groups. The resulted material, **MDAF-6-NH$_3$**, shows five orders of magnitude enhancement in proton conductivity compared to **MDAF-6** in saturated NH_3-H_2O vapor, indicating the importance of the coexistence of NH_4^+-NH_3 and H_3O^+-H_2O conjugate acid-base pairs for proton conduction (Scheme 1). The magnetic properties of **MDAF-6** were also studied.

Compound **MDAF-6** was obtained as pale-yellow rhombus crystals after solvothermal reaction of $DyCl_3{\cdot}6H_2O$, amp_2H_4 and mal-

* Corresponding author.
E-mail address: lmzheng@nju.edu.cn (L.-M. Zheng).
[1] These authors contributed equally to this work.

https://doi.org/10.1016/j.cclet.2023.108320
1001-8417/

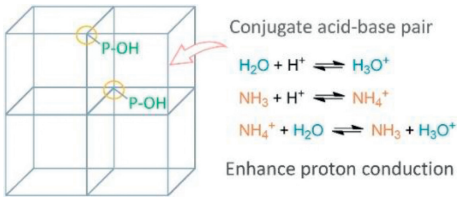

Scheme 1. The framework of **MDAF-6** containing P-OH for NH_3 and H_2O adsorption.

onic acid in CH_3OH/H_2O at 90 °C for 48 h, and was characterized by PXRD, TG and IR measurements (Figs. S1–S3 in Supporting information). Single crystal structural analysis revealed that it crystallizes in the orthorhombic system, polar space group $Pmn2_1$ (No. 31) (Table S1 in Supporting information). The asymmetric unit contains two kinds of Dy atoms (each with half occupancy), one $amp_2H_2^{2-}$ ligand, half an occupied malonate, one coordinated and 2.5 lattice water molecules (Fig. S4 in Supporting information). The lattice water molecules were treated with PLATON/SQUEEZE program because of heavy disorder, and the number was determined by elemental and thermal analyses (Fig. S2 in Supporting information). Both Dy atoms reside on the mirror plane, and each is seven-coordinated by four O atoms from four $amp_2H_2^{2-}$ ligands (O1, O1A, O5B and O5C for Dy1; O2, O2A, O4D and O4E for Dy2), two O atoms from the chelated malonate anion (O7 and O9 for Dy1; O7 and O8 for Dy2), and one from water molecule (O1W for Dy1; O2W for Dy2) (Fig. 1a). The Dy-O bond lengths and O-Dy-O angles are 2.218(9)–2.465(16) Å and 69.2(2)°–156.4(4)° for Dy1, and 2.232(9)–2.749(9) Å and 50.5(3)°–167.0(4)° for Dy2 (Table S2 in Supporting information). The $\{DyO_7\}$ core has a distorted capped trigonal prism geometry (CShM = 0.755 for Dy1 and 1.434 for Dy2, Table S3 in Supporting information) [37]. The adjacent Dy1 and Dy2 atoms are connected alternatively by triple bridges of two O-P-O and one μ-O and double bridges of O-P-O units (Dy1···Dy2 distance: 4.558, 5.389 Å), forming an infinite polar chain running along the *b*-axis, where the disordered malonate ligands locate on the same side (Fig. 1b). Each $amp_2H_2^{2-}$ serves as a tetradentate ligand binding to four Dy atoms, whereas each mal^{2-} also acts as a tetradentate ligand chelating and bridging the Dy1 and Dy2 atoms (Fig. S5 in Supporting information). The neighboring chains are cross-linked by the $amp_2H_2^{2-}$ ligands forming a 3D framework structure (Fig. 1c). A 1D channel is generated along the *b*-axis with the window dimension of *ca.* 7.0 × 6.2 $Å^2$ (van der Waals radii not accounted). It is noted that one of the two protonated phosphonate oxygen atom (O6) forms intrachain H-bond with the malonate oxygen atom O8, while the other (O3) points towards the channel center, and should form H-bond with lattice water molecule. Thus, the channel wall is hydrophobic on the dianthracene side, but hydrophilic on the chain side with pendent P-OH, malonate oxygen atom, and coordination water molecules.

To examine the stability of **MDAF-6**, the crystalline sample was immersed in water with different pH (1–14) for 24 h at room temperature. The PXRD measurements confirmed the stability of the material at pH 2–12 (Fig. S6 in Supporting information). Thermal analysis revealed that **MDAF-6** lost seven water molecules below 170 °C (obs. 7.2%, calcd. 7.7%). The weight loss above 170 °C is due to the decomposition of organic components and the collapse of the framework structure (Fig. S2).

We next investigated the adsorption/desorption performance of **MDAF-6**, activated under vacuum at 100 °C for 4 h (weight loss: obs. 7.8%, calcd. 7.7%), toward N_2, CO_2, NH_3 and H_2O gasses (Fig. 1d). The N_2 adsorption/desorption isotherm at 77 K is a Type II isotherm with a small loading of 4.1 cm^3/g at $P/P_0 = 0.98$, indicating a very weak interaction between nitrogen and pore walls. The adsorption was increased for CO_2 at 298 K with a maximum uptake of 23.6 cm^3/g (1.6 mol/mol) at $P/P_0 = 0.98$. A quick and dramatically enhanced adsorption was found for NH_3 with uptakes of 92.0 cm^3/g (6.1 mol/mol) at $P/P_0 = 0.04$ and 142.4 cm^3/g (9.4 mol/mol, 6.35 mmol/g) at $P/P_0 = 0.98$ at 298 K, attributed to the favourable acid-base interaction between P-OH and NH_3. The capacity is higher than MIL-53 (4.40 mmol/g) but lower than NH_2−MIL-53 and MIL-100 (8.00 mmol/g) [38]. After desorption, there remained 75.0 cm^3/g (4.9 mol/mol) of ammonia at $P/P_0 = 0.001$, which is higher than the expected value of 4.0 mol^{-1} when all four P–OH groups per molecular formula interacted with NH_3 to form non-volatile PO_3^{2-}-NH_4^+ pairs. This result suggests that NH_3 may also occupy the vacancy left by the Dy atom after removing the coordination water. The formation of PO_3^{2-}-NH_4^+ pair

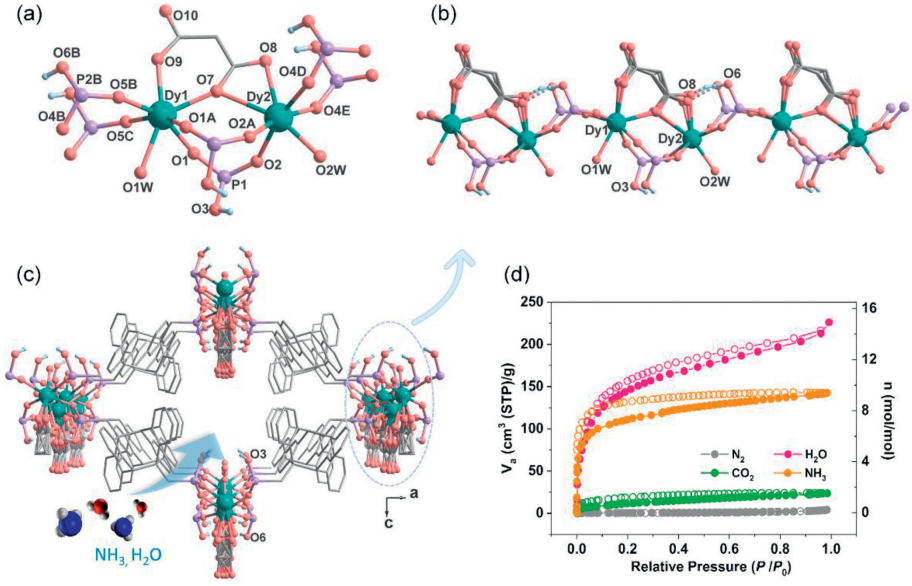

Fig. 1. (a) Building unit of **MDAF-6**. Part of the disordered malonate and the organic group of $amp_2H_2^{2-}$ ligand are omitted for clarity. (b) The infinite chain in **MDAF-6** running along the *b*-axis. (c) The open framework structure of **MDAF-6** viewed along the *b*-axis. All H atoms except for those attached to phosphonate oxygen atoms are omitted for clarity. (d) The adsorption (filled) and desorption (open) isotherms for solvent-free **MDAF-6**: N_2 (77 K), CO_2 (298 K), NH_3 (298 K) and water vapor (298 K).

breaks the intrachain H-bond between P-OH and malonate oxygen and weakens the O(P)-H bond, and thus should increase the proton concentration for conduction in the framework channel. The sample after adsorption/desorption of NH_3 at 298 K is named as **MDAF-6-NH$_3$**. Interestingly, the re-activated sample, after heating **MDAF-6-NH$_3$** at 150 °C under vacuum for 10 min (weight loss: obs. 5.8%, calcd. 5.6%), showed similar capacity of NH_3 adsorption at P/P_0 =1.0 (Fig. S7 in Supporting information).

The water adsorption isotherm of the fully dehydrated sample of **MDAF-6** showed a quick uptake of water vapor, and the value reached 118.7 cm^3/g (7.8 mol/mol) at $P/P_0 = 0.08$ and 226 cm^3/g (15 mol/mol) at $P/P_0 = 0.99$ at 298 K (Fig. S8 in Supporting information). When desorbed, there were still about 100.3 cm^3/g (7 mol/mol) H_2O in the structure at $P/P_0 = 0.03$, in agreement with the presence of two coordinated and five lattice water molecules. We also measured the water adsorption capacity of **MDAF-6-NH$_3$** at 298 K and observed an uptake of 78.4 cm^3/g (5.3 mol/mol) at $P/P_0 = 0.96$, which is much lower than that for **MDAF-6** (14.5 mol/mol). This is reasonable because the channel space in **MDAF-6-NH$_3$** is partially filled with the loaded NH_3 molecules. In addition, the hysteresis of water adsorption/desorption isotherm is more significant for **MDAF-6-NH$_3$** than for **MDAF-6**, indicating a strong interaction between water and NH_4^+/NH_3. Notably, the water adsorption capacity of **MDAF-6** and **MDAF-6-NH$_3$** drops significantly upon slight increase of temperature. At 308 K, the capacities became 179.8 cm^3/g (11.8 mol/mol) for **MDAF-6** at $P/P_0 = 0.98$ and 67.1 cm^3/g (4.4 mol/mol) for **MDAF-6-NH$_3$** at $P/P_0 = 1.00$, respectively (Fig. S9 in Supporting information).

The proton conductivity (σ) of **MDAF-6** and **MDAF-6-NH$_3$** was evaluated by impedance spectroscopy measurements using a pellet sample placed in a temperature and humidity-controlled chamber for 12 h. For **MDAF-6**, the conductivity at 298 K was 1.8×10^{-12} S/cm at 40% RH and increased to 1.5×10^{-9} S/cm at 95% RH (Fig. 2a and Fig. S10 in Supporting information). The values are very low compared to other proton conductive metal phosphonates with protonated phosphonate groups [22]. From the structure of **MDAF-6**, we can see that hydrophobic dianthracene moieties are present in the channel which is unfavorable for the formation of continuous hydrogen bond network. Besides, half of the protonated P-OH groups participate in strong intrachain hydrogen bonds, which may 'freeze' the protons, prevent them from migration, and thus affect their conduction. The adsorption of ammonia lifted the freeze of protons due to the acid-base interaction between P-OH and NH_3 to form NH_4^+ in **MDAF-6-NH$_3$**. Proton conductivity measurements at 298 K revealed a remarkably improved conductivity of 1.0×10^{-10} S/cm at 40% RH and 6.8×10^{-6} S/cm at 95% RH (Fig. 2a and Fig. S11 in Supporting information). The latter is three orders of magnitude higher than that for **MDAF-6**. This value is comparable to some metal-triphosphonates [22,39], but lower than a few 3D metal-tetraphosphonates (*ca.* 10^{-2}–10^{-4} S/cm) [26,40,41]. Obviously, the NH_4^+ ions formed *in-situ* promote the water-mediated proton conduction.

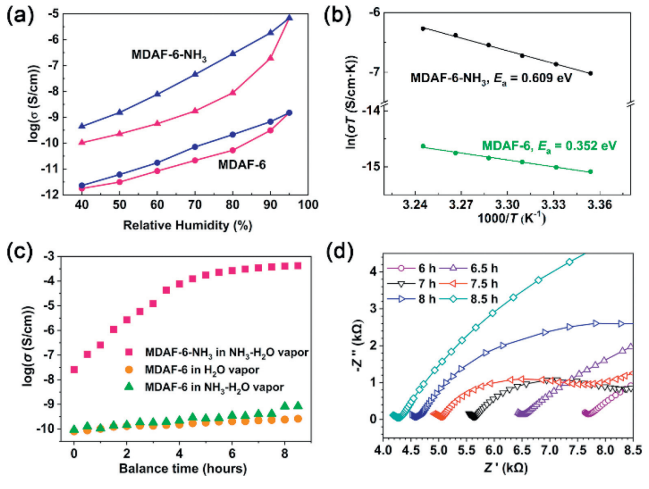

Fig. 2. (a) Proton conductivities of **MDAF-6** and **MDAF-6-NH$_3$** from 40% to 95% RH at 298 K (pink for increasing RH and blue for decreasing RH). (b) Arrhenius plot of the temperature dependence at 95% RH for **MDAF-6** (green) and **MDAF-6-NH$_3$** (black). (c) Proton conductivities of **MDAF-6-NH$_3$** in ammonia vapor, **MDAF-6** in water vapor and **MDAF-6** in ammonia vapor. (d) Nyquist plots of **MDAF-6-NH$_3$** in ammonia vapor for 6–8.5 h.

To confirm this, we first evaluated the proton conductivity of **MDAF-6-NH$_3$** under a dry NH_3 gas atmosphere at 100 kPa. The sample pellet was dried at 100 °C under vacuum for activation using a hot stage with electrical probes and then filled with dry NH_3 gas after cooling to room temperature. After being exposed to NH_3 gas for about 7 h, the gas adsorption of the sample pellet reached equilibrium and exhibited a conductivity of 3.4×10^{-9} S/cm at 304 K (Fig. S13 in Supporting information). This value is higher than that obtained at 298 K and 40% RH (1.0×10^{-10} S/cm), but much lower than that obtained at 298 K and 95% RH. The result indicates that the filling of NH_3 gas is not sufficient to form a continuous hydrogen bond network for efficient proton conduction. We then exposed the same pellet of **MDAF-6-NH$_3$** to saturated NH_3-H_2O vapor. Interestingly, the proton conductivity drastically increased along with prolonged time and reached a maximum value of *ca.* 4.2×10^{-4} S/cm after 8.5 h (Figs. 2c and d, Fig. S14 in Supporting information). Controlled experiments were carried out under the same conditions for **MDAF-6** in water or NH_3-H_2O vapor. As shown in Fig. 2c, the proton conductivity of **MDAF-6** was *ca.* 10^{-9} S/cm after exposure to water or NH_3-H_2O vapor for 8.5 h, which is 5 orders of magnitude lower than that for **MDAF-6-NH$_3$**. The conductivity of **MDAF-6** reached the equilibrium value of 2.1×10^{-8} S/cm after 32 h exposure to water vapor, and 6.9×10^{-5} S/cm after 172 h exposure to NH_3-H_2O vapor (Fig. S15 in Supporting information). Notably, the framework structure of **MDAF-6** remained the same after thermal treatment, the NH_3 gas adsorption/desorption process, and exposure to saturated NH_3-H_2O vapor (Fig. S16 in Supporting information).

The above results showed that the water-mediated proton productivity of **MDAF-6** was significantly enhanced after the incorporation of NH_4^+. In this case, there exist two acid-base pairs, *e.g.*, H_3O^+-H_2O and NH_4^+-H_2O, which participate in the proton conduction pathway. We postulate that the presence of conjugate acid-base pair of NH_4^+-NH_3 would facilitate the proton mobility.

The temperature-dependent proton conductivities of **MDAF-6** and **MDAF-6-NH$_3$** were measured at 95% RH. The proton conductivities were almost unchanged for both compounds when the temperature went up to 35 °C and further reduced above 35 °C (Fig. S12 in Supporting information), in consistence with the partial release of water molecules at this temperature. Based on the data in the temperature decreasing process, the activation energies (E_a) were estimated to be 0.35 eV for **MDAF-6** and 0.61 eV for **MDAF-6-NH$_3$** (Fig. 2b). The larger E_a (>0.6 eV) suggests that NH_4^+ may migrate directly as a proton attached to a vehicle in **MDAF-6-NH$_3$**.

To understand the mechanism of enhanced proton conductivity of **MDAF-6-NH$_3$** in NH_3-H_2O vapor, we measured the solid-state IR and ^1H MAS NMR spectra of the samples. Fig. S3 shows the IR spectra of **MDAF-6** and **MDAF-6-NH$_3$**. Compared to **MDAF-6** (3619, 3522 and 3441 cm^{-1}), the O-H stretching vibrations of **MDAF-6-NH$_3$** are red-shifted to 3603, 3499 and 3418 cm^{-1}, indicating the weakening of the O-H stretching vibration. In addition, there appears a new broad peak at 3196 cm^{-1}, attributed to the N-H stretching vibration. The P-O stretching vibrations are very different for the two samples with additional strong peaks appearing

at 1042 and 1001 cm^{-1} for **MDAF-6-NH_3**. These results corroborate with the fact that the P-OH acidic group reacted with NH_3 base forming PO_3^{2-}-NH_4^+ pair in **MDAF-6-NH_3**.

After exposure to NH_3-H_2O vapor for 8.5 h, both **MDAF-6** and **MDAF-6-NH_3** show broad bands at 3680–3280 cm^{-1}, ascribed to the presence of extensive hydrogen bonding networks (Fig. S17 in Supporting information). Compared to **MDAF-6**, **MDAF-6-NH_3** shows an enhanced stretching vibration at *ca.* 3435 cm^{-1} and additional bands at 3207, 1402 and 1207 cm^{-1}. The latter three peaks are attributed to the N-H vibrations of NH_4^+ and NH_3 [42,43]. The broad N-H stretching peak at 3207 cm^{-1} may be related to the formation of hydrogen bonds between NH_3 and NH_4^+ [44]. The observation of these N-H vibrations for **MDAF-6-NH_3** but not for **MDAF-6** indicates that **MDAF-6-NH_3** adsorbs NH_3-H_2O vapor quickly and reaches equilibrium within 8.5 h. By contrast, **MDAF-6** adsorbs NH_3-H_2O vapor slowly and needs much longer time (*ca.* 172 h) to reach equilibrium. This fact gives us an opportunity to distinguish the role of the NH_4^+-NH_3 conjugate pair in proton conduction. For **MDAF-6** exposed to NH_3-H_2O or pure water vapor, there was negligible or no NH_4^+-NH_3 conjugate pair generated within 8.5 h, and their conductivities were extremely low (*ca.* 10^{-9} S/cm^2). Therefore, the significantly enhanced proton conductivity of **MDAF-6-NH_3** in saturated NH_3-H_2O vapor (*ca.* 10^{-4} S/cm^2) has to contribute to the coexistence of the NH_4^+-NH_3 and H_3O^+-H_2O conjugate pairs.

We also measured the solid-state ^1H MAS NMR spectra of the above three samples. As shown in Fig. S18 (Supporting information), a resonance signal appears at 4.2 ppm for **MDAF-6** exposed to H_2O and NH_3-H_2O vapor for 8.5 h, corresponding to physisorbed water moving freely in the pore system of the material [45]. For **MDAF-6-NH_3** exposed to NH_3-H_2O vapor for 8.5 h, the signal is slightly shifted to 5 ppm, which could be related to the presence of NH_4^+(NH_3) and H_2O interactions.

Based on the above results, we propose the mechanism of proton conduction of **MDAF-6-NH_3** in NH_3-H_2O vapor as below: (1) The formation of PO_3^{2-}-NH_4^+ pair breaks the intrachain H-bond between P-OH and malonate oxygen and weakens the O(P)-H interaction, thus increasing the proton concentration for conduction; (2) The NH_4^+ ion forms H-bonds with neutral NH_3 and transfers proton with low energy barrier [44]; (3) Saturated NH_3-H_2O atmosphere provides a continuous network of H-bonds for efficient proton conduction (Scheme 2).

In order to explore the possibility of using **MDAF-6** as a magnetic proton conductor [46,47], we also investigated its magnetic properties. As shown in Fig. S19 (Supporting information), the $\chi_M T$ value of **MDAF-6** (28.17 cm^3 K/mol per Dy_2) at room temperature agrees well with the spin-only value of 28.34 cm^3 K/mol for two isolated Dy^{III} ions ($^6H_{15/2}$, $S = 5/2$, $L = 5$, $g_J = 4/3$). The $\chi_M T$ decreases progressively upon cooling, attributed to the thermal depopulation of Dy^{III} Stark sublevels and possible weak antiferromagnetic interactions. Field-dependent magnetization measured from 2 K to 10 K showed unsaturation up to 70 kOe (Fig. S19, inset), suggesting the presence of magnetic anisotropy and/or lower lying excited states. The alternating current (ac) susceptibility data of **MDAF-6** revealed a frequency dependence of the out-of-phase (χ") signals under zero or 1 kOe dc field (Fig. S20 in Supporting information), characteristic of single-molecule magnet (SMM) behavior. But no maximum was observed, thus excluding the possibility to derive the energy barrier of the material.

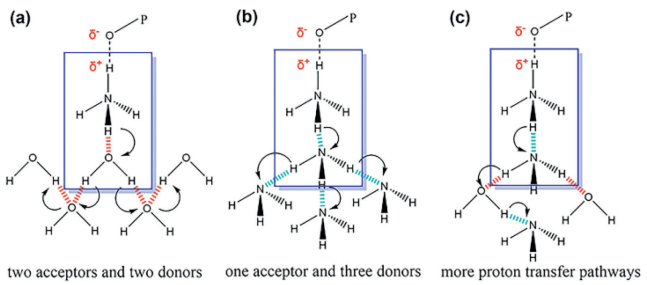

Scheme 2. Proposed proton transfer pathways of **MDAF-6-NH_3** in (a) water, (b) NH_3 and (c) NH_3-H_2O atmosphere.

In summary, we report a new porous dysprosium phosphonate framework $Dy_2(amp_2H_2)_2(mal)(H_2O)_2{\cdot}5H_2O$ (**MDAF-6**) which shows a high adsorption capacity toward NH_3 due to the presence of P-OH acidic groups. Impressively, we observed a dramatic enhancement of proton conductivity after exposing **MDAF-6-NH_3** in saturated NH_3-H_2O vapor, demonstrating the importance of coexistent conjugate acid-base pairs of H_3O^+-H_2O and NH_4^+-NH_3 in promoting proton conduction. In addition, **MDAF-6** shows SMM behavior at low temperature. This work not only provides a new example of proton conductive magnetic materials, but also a new approach to boost the proton conduction of MOFs by introducing conjugated acid-base pairs of H_3O^+-H_2O and NH_4^+-NH_3 in NH_3-H_2O media.

Declaration of competing interest

The authors declare that they have no known competing financial interests or personal relationships that could have appeared to influence the work reported in this paper.

Acknowledgments

This work was supported by grant from the National Natural Science Foundation of China (No. 21731003).

Supplementary materials

Supplementary material associated with this article can be found, in the online version, at doi:10.1016/j.cclet.2023.108320.

References

[1] D.W. Lim, H. Kitagawa, Chem. Rev. 120 (2020) 8416–8467.
[2] Y.X. Ye, L.S. Gong, S.C. Xiang, Z.J. Zhang, B.L. Chen, Adv. Mater. 32 (2020) 1907090.
[3] S.C. Pal, M.C. Das, Adv. Funct. Mater. 31 (2021) 2101584.
[4] M. Sadakiyo, H. Kitagawa, Dalton Trans. 50 (2021) 5385–5397.
[5] A.L. Li, Q. Gao, J. Xu, X.H. Bu, Coord. Chem. Rev. 344 (2017) 54–82.
[6] L.L. Kang, M. Xue, Y.Y. Liu, G. Li, et al., Coord. Chem. Rev. 452 (2022) 214301.
[7] Y.R. Liu, Y.Y. Chen, Q. Zhuang, G. Li, Coord. Chem. Rev. 471 (2022) 214740.
[8] D.A. Levenson, J. Zhang, P.M.J. Szell, et al., Chem. Mater. 32 (2020) 679–687.
[9] H. Wang, Q. Wu, X. Ding, et al., Inorg. Chem. 59 (2020) 8361–8368.
[10] J. Hu, H. Zhang, Z. Feng, et al., Chin. Chem. Lett. 33 (2022) 3227–3230.
[11] Y. Xu, S.L. Yang, G. Li, et al., Chem. Mater. 34 (2022) 5500–5510.
[12] Y.X. Lian, S.S. Liu, J.J. Sun, et al., Dalton Trans. 51 (2022) 14054–14058.
[13] D.W. Lim, M. Sadakiyo, H. Kitagawa, Chem. Sci. 10 (2019) 16–33.
[14] D.W. Lim, H. Tsukada, A. Shigematsu, et al., ChemRxiv (2018), https://doi.org/10.26434/chemrxiv.7319273.v1.
[15] X. Liang, B. Li, M. Wang, et al., ACS Appl. Mater. Interfaces 9 (2017) 25082–25086.
[16] R.L. Liu, L.L Zhao, W. Dai, et al., Inorg. Chem. 57 (2018) 1474–1482.
[17] Q.Q. Liu, S.S. Liu, X.F. Liu, et al., Inorg. Chem. 61 (2022) 3406–3411.
[18] I.R. Salcedo, M. Bazaga-García, R.M.P. Colodrero, et al., Dalton Trans. 49 (2020) 3981–3988.
[19] Y.J. Wang, J.B. Yin, D. Liu, et al., J. Mater. Chem. A 9 (2021) 2683–2688.
[20] A. Clearfield, K. Demadis, Metal Phosphonate Chemistry: from Synthesis to Applications, Royal Society of Chemistry, Cambridge, 2012.
[21] K.J. Gagnon, H.P. Perry, A. Clearfield, Chem. Rev. 112 (2012) 1034–1054.
[22] S.S. Bao, G.K.H. Shimizu, L.M. Zheng, Coord. Chem. Rev. 378 (2019) 577–594.
[23] S.S. Bao, M.F. Qin, L.M. Zheng, Chem. Commun. 56 (2020) 12090–12108.
[24] R.F. Mendes, P. Barbosa, E.M. Domingues, et al., Chem. Sci. 11 (2020) 6305–6311.
[25] Y.Y. Enakieva, E.A. Zhigileva, A.N. Fitch, et al., Dalton Trans. 50 (2021) 6549–6560.
[26] M.F. Qin, C.Y. Wang, S.S. Bao, L.M. Zheng, Chem. Commun. 58 (2022) 8372–8375.

[27] Q. Zou, T. Shang, X.D. Huang, et al., J. Mater. Chem. C 9 (2021) 10749–10758.
[28] Q. Zou, S.S. Bao, X.D. Huang, et al., Chem. Asian J. 16 (2021) 1456–1465.
[29] Q. Zou, G.L. Wang, Y.Q. Chen, et al., Chem. Eur. J. 29 (2023) e202203454.
[30] L. Qin, Y.Z. Yu, P.Q. Liao, et al., Adv. Mater. 28 (2016) 10772–10779.
[31] J.J. Hu, Y.G. Li, H.R. Wen, et al., Inorg. Chem. 61 (2022) 6819–6828.
[32] S.P. Bera, A. Mondal, S. Roy, et al., Dalton Trans. 47 (2018) 15405–15415.
[33] S.P. Bera, A. Mondal, S. Konar, Chem. Asian J. 14 (2019) 3702–3711.
[34] S.M. Elahi, Q.H. Lai, M. Ren, et al., Inorg. Chem. 58 (2019) 14034–14045.
[35] Q. Zhang, J.X. Hu, Q. Li, et al., Chin. Chem. Lett. 33 (2022) 1417–1421.
[36] Y.B. Lu, J. Huang, Y.Q. Liao, et al., Inorg. Chem. 61 (2022) 18545–18553.
[37] M. Pinsky, D. Avnir, Inorg. Chem. 37 (1998) 5575–5582.
[38] D.W. Kang, S.E. Ju, D.W. Kim, et al., Adv. Sci. 7 (2020) 2002142.
[39] X.L. Huang, Y.Q. Chen, G.H. Wen, S.S. Bao, L.M. Zheng, CrystEngComm 24 (2022) 3886–3893.
[40] D. Chakraborty, A. Ghorai, A. Chowdhury, S. Banerjee, A. Bhaumik, Chem. Asian J. 16 (2021) 1562–1569.
[41] Y.Y. Enakieva, A.A. Sinelshchikova, M.S. Grigoriev, et al., Chem. Eur. J. 27 (2021) 1598–1602.
[42] K.J. Frink, R.C. Wang, J.L. Colón, A. Clearfield, Inorg. Chem. 30 (1991) 1438–1441.
[43] Z.G. Huang, Z.Y. Liu, X.L. Zhang, Q.Y. Liu, Appl. Catal. B: Environ. 63 (2006) 260–265.
[44] L. Rosso, M.E. Tuckerman, Solid Sate Ion. 161 (2003) 219–229.
[45] J.V. Aelst, M. Haouas, E. Gobechiya, et al., J. Phys. Chem. C 118 (2014) 22573–22582.
[46] C. Zhang, X. Ma, P. Cen, et al., Dalton Trans. 49 (2020) 14123–14132.
[47] W. Gao, H. Huang, A.M. Zhou, et al., CrystEngComm 22 (2020) 267–274.